Available online at www.sciencedirect.com
ScienceDirect
Journal of Catalysis 248 (2007) 303–310
JOURNAL OF CATALYSIS
www.elsevier.com/locate/jcat

The modification effect of Fe on amorphous CoB alloy catalyst for chemoselective hydrogenation of crotonaldehyde

Yan Pei [a], Pingjun Guo [a], Minghua Qiao [a,*], Hexing Li [b], Shiqiang Wei [c], Heyong He [a], Kangnian Fan [a,*]

[a] *Department of Chemistry and Shanghai Key Laboratory of Molecular Catalysis and Innovative Materials, Fudan University, Shanghai 200433, PR China*
[b] *Department of Chemistry, Shanghai Normal University, Shanghai 200234, PR China*
[c] *National Synchrotron Radiation Laboratory, University of Science and Technology of China, Hefei 230029, PR China*

Received 11 December 2006; revised 13 February 2007; accepted 25 March 2007

Abstract

Binary CoB and ternary CoFeB amorphous alloy catalysts with different Fe contents were prepared by the chemical reduction method. In liquid-phase hydrogenation of crotonaldehyde, incorporation of Fe into the CoB catalyst reduced the overall activity while effectively improving the selectivity and yield to crotyl alcohol. On the optimum CoFeB-3 catalyst with a nominal Fe/(Co + Fe) molar ratio of 0.6, the initial selectivity amounted to 71%, and the yield of crotyl alcohol reached 63%. It is found that the selectivity enhancement was due to the lower decrement in the intrinsic formation rate of crotyl alcohol compared with that of butanal, not to the increment in the activation of the C=O bond. Based on the characterizations, including X-ray photoelectron spectroscopy and X-ray absorption spectroscopy, and previous findings, the enhanced selectivity from Fe modification was tentatively attributed to an ensemble size effect.
© 2007 Elsevier Inc. All rights reserved.

Keywords: CoB; Fe modification; Amorphous alloy; Crotonaldehyde; Crotyl alcohol; Hydrogenation; Ensemble size effect

1. Introduction

Selective hydrogenation of crotonaldehyde to the unsaturated crotyl alcohol is of commercial interest in pharmaceutical and fragrance production. The reaction also is of great scientific importance, because the saturated aldehyde butanal is thermodynamically favored and usually also kinetically favored on monometallic catalysts [1–3]. Selectivity manipulation is generally achieved by supporting the monometallic catalysts on an oxide, which can lower the antibonding π^*_{CO} orbital of the C=O bond, facilitating better backdonation from the metal orbitals [4,5], or by interacting with a second, more electropositive metal [6,7], which can increase the electron density on the active site, thus repelling the adsorption of the α,β-unsaturated aldehyde through the C=C bond [8].

Since the 1980s, metal boride amorphous alloy catalysts prepared by reduction of metal salts with borohydride have attracted much attention in catalysis owing to their unique properties, such as isotropic structure and high concentration of coordinatively unsaturated sites [9–12]. The amorphous CoB alloy catalyst is a promising candidate for the selective hydrogenation of α,β-unsaturated aldehydes to unsaturated alcohols [13–17]. In line with the findings on crystalline monometallic catalysts, modification with an oxide [16] or a metal salt [13,17] is crucial to enhanced selectivity of the amorphous CoB catalyst. On the other hand, only limited work has been carried out to investigate the effect of a reducible second metal on the catalytic performance of the CoB catalyst. For example, we have found that the selectivity to crotyl alcohol over the ternary CoSnB amorphous catalyst is inferior to that achieved by directly adding the corresponding metal salt with crotonaldehyde during hydrogenation [18].

Recently, we developed a Fe-modified CoB amorphous alloy catalyst retaining high selectivity toward crotyl alcohol even

* Corresponding authors. Fax: +86 21 65642978.
E-mail addresses: mhqiao@fudan.edu.cn (M. Qiao), knfan@fudan.edu.cn (K. Fan).

0021-9517/$ – see front matter © 2007 Elsevier Inc. All rights reserved.
doi:10.1016/j.jcat.2007.03.024

at nearly complete conversion of crotonaldehyde. A brief report on the excellent selectivity of this CoFeB catalyst has been published elsewhere [19]. In this paper, we present a detailed characterization with special emphasis on the modification effect of Fe on the structural and electronic properties of the amorphous CoB catalyst, based on which the possible modification mechanism of Fe on the CoB catalyst in liquid-phase hydrogenation of crotonaldehyde is discussed.

2. Experimental

2.1. Catalyst preparation

The CoB catalyst was prepared by the chemical reduction method. First, 12.7 ml of a KBH_4 aqueous solution (2.0 M, with 0.2 M NaOH) was added at a flow rate of 1.5 ml min^{-1} to 17.0 ml of a $CoCl_2$ aqueous solution (0.59 M) at 293 K under gentle stirring. When no more hydrogen bubbles were released, the black precipitate was centrifuged and washed six times with distilled water, then three times with ethanol.

The ternary CoFeB catalyst was prepared following an identical procedure, except that the desired amount of $FeCl_3$ was mixed with the $CoCl_2$ solution before KBH_4 reduction, with the total amount of $CoCl_2$ and $FeCl_3$ maintained at 0.01 mol. The nominal Fe/(Co + Fe) molar ratios were 0.2, 0.4, and 0.6, and the corresponding catalysts were designated CoFeB-1, CoFeB-2, and CoFeB-3. For comparison, a FeB catalyst was prepared using an aqueous solution containing only $FeCl_3$ under the same condition. The foregoing catalysts were stored in ethanol for activity testing and characterization. No further treatment was performed before catalytic testing.

2.2. Characterization

The bulk compositions of the as-prepared catalysts were analyzed by inductively coupled plasma-atomic emission spectroscopy (ICP-AES; Thermo Elemental IRIS Intrepid). N_2 physisorption at 77 K was performed on a Micromeritics TriStar3000 apparatus. A sample stored under ethanol was transferred to the adsorption glass tube and heated at 383 K under N_2 for 2 h before measurement. The weight of the sample was determined by the difference in the adsorption tube on completion of the experiment.

H_2 chemisorption was determined using temperature-programmed desorption (TPD). After heating at 423 K for 1.5 h under Ar, the sample was cooled to room temperature. Then H_2 was introduced instead of Ar for 1.0 h to ensure saturation adsorption of H_2. The sample was then purged with Ar to remove the gaseous and/or physisorbed hydrogen until the TCD signal returned to the baseline. The maximum desorption temperature of 873 K was achieved at a heating rate of 20 K min^{-1}. The TPD curve was integrated, and the number of moles of desorbed H_2 was determined by comparing its area with the area of a calibrated hydrogen pulse. The total metal surface area (S_H) of the catalyst was calculated based on the assumption of a H:Co(Fe) stoichiometry of 1:1 [20]. The pulsed adsorption method was not used here because there is residual H_2 on the sample arising from H_2 released during sample preparation. Thorough elimination of the preadsorbed H_2 for the pulsed H_2 adsorption experiment requires high temperature (>750 K), as indicated by H_2-TPD, which would inevitably deteriorate the amorphous structure of the sample with crystallization temperature around 493 K.

Powder X-ray diffraction (XRD) patterns were acquired on a Bruker AXS D8 Advance X-ray diffractometer using Ni-filtered Cu$K\alpha$ radiation ($\lambda = 0.15418$ nm) coupled to a high-temperature cell purging with N_2 to avoid exposure of the catalysts to air. The tube voltage was 40 kV, and the current was 40 mA. The surface morphology and particle size were measured by transmission electron microscopy (TEM) using a JEOL JEM2011 microscope. The amorphous structure of the catalysts was detected by selected-area electron diffraction (SAED).

X-ray absorption spectroscopy (XAS) data were measured for the Co K-edge in the transmission mode at room temperature at the U7C beam line of the National Synchrotron Radiation Laboratory (NSRL, Hefei). The typical electron beam energy was 0.8 GeV, and the current was 160 mA. The fixed-exit Si(111) flat double-crystal monochromator was detuned to 70% of the maximum intensity to avoid higher harmonics. The sample with storage liquid was sealed with Scotch tape and inserted in the sample plate. X-ray absorption near-edge structure (XANES) spectra were compared after normalization. The extended X-ray absorption fine-structure (EXAFS) spectra were analyzed by the NSRLXAFS 3.0 package compiled by NSRL according to standard procedures [21]. For disordered systems, the symmetric Gaussian pair distribution function is invalid for the nearest neighbor atom distribution, so a convolution of Gaussian and exponent function was used to derive the EXAFS formula [22]. Theoretical backscattering amplitudes and phase shifts for the Co–Co/Fe and Co–B pairs were calculated using the FEFF8.20 code [23] with hcp-Co and Co_2B as the reference compounds, respectively.

X-ray photoelectron spectroscopy (XPS) was done using a PerkinElmer PHI5000C instrument with Mg$K\alpha$ radiation as the excitation source ($h\nu = 1253.6$ eV). The sample was pressed into a self-supported disc and mounted on the sample plate. It was degassed in the pretreatment chamber at 298 K for 4 h in vacuo before being transferred to the analyzing chamber, in which the background pressure was $<2 \times 10^{-9}$ Torr. The spectra were recorded after Ar^+ sputtering of the surface for 15 min. All binding energy (BE) values were referenced to the C 1s peak of contaminant carbon at 284.6 eV with an uncertainty of ±0.2 eV.

2.3. Catalytic testing

Crotonaldehyde was purified by distillation before catalytic testing. Liquid-phase hydrogenation of crotonaldehyde was carried out in a 220-mL stainless steel autoclave in which 0.50 g of catalyst, 5.0 ml of crotonaldehyde, and 45.0 ml of ethanol were loaded. The reactor was purged with N_2, followed by H_2. After the desired temperature (373 K) was reached, the H_2 pressure was raised to 1.0 MPa and stirring (1000 rpm) was commenced;

Table 1
Physicochemical properties of the CoB and CoFeB catalysts

Catalyst	Fe/(Co + Fe) (mol%)		Bulk comp. (atomic ratio)	S_{BET} ($m^2\ g^{-1}$)	d[a] (nm)	S_H[b] ($m^2\ g_{cat}^{-1}$)
	Nominal	Exp.				
CoB	0	0	$Co_{65.6}B_{34.4}$	18	16	15
CoFeB-1	20.0	20.1	$Co_{54.2}Fe_{13.6}B_{32.2}$	27	9	13
CoFeB-2	40.0	36.2	$Co_{43.8}Fe_{24.9}B_{31.3}$	32	8	10
CoFeB-3	60.0	54.6	$Co_{30.8}Fe_{37.1}B_{32.1}$	35	7	9
FeB	100	100	$Fe_{77.9}B_{22.1}$	42	–	–

[a] d, particle size diameter, determined by TEM.
[b] Calculated from the amount of H_2 desorbed after saturation adsorption of H_2.

this was considered the beginning of the reaction. The reaction was monitored by analyzing samples withdrawn from the autoclave at intervals on a GC122 gas chromatograph equipped with a 30-m PEG-20M capillary column and a flame ionization detector. The initial hydrogenation rate of crotonaldehyde increased proportionally to the catalyst weight (0.2–1.0 g) when other reaction conditions were fixed, confirming the absence of any transport limitations.

3. Results and discussion

3.1. Bulk composition, surface area, and morphology

Table 1 lists the bulk compositions and specific surface areas of the CoB, CoFeB, and FeB catalysts. It shows that the bulk Fe/(Co + Fe) ratio in the CoFeB catalysts closely mimics the nominal Fe/(Co + Fe) ratio, with >90% of Fe incorporated into the catalysts. Incorporation of Fe into the CoB catalyst improved the BET surface area, which increased steadily from 18 $m^2\ g^{-1}$ for CoB to 42 $m^2\ g^{-1}$ for FeB (Table 1). However, the BET surface area exhibited an exponential decay rather than a linear relationship with the bulk Fe content, indicating the formation of ternary CoFeB alloys rather than a mechanical mixture of the CoB and FeB alloys.

The TEM images of the CoB catalyst shows that the catalyst was composed of spherical particles ca. 16 nm in diameter (Fig. 1a). Aggregation due to the high surface energy of the CoB nanoparticles was observed. Incorporating Fe reduced the particle size, as shown in Figs. 1b–1d. The average diameter was reduced to ca. 9 nm for CoFeB-1, and kept on decreasing at higher Fe content. With the assumption of a spherical shape and nonporous texture of the nanoparticles, a simple calculation revealed that the ratio between the surface areas was the inverse of the ratio between their corresponding particle sizes, as confirmed by the data given in Table 1. Figs. 1b–1d also show that the incorporation of Fe led to better dispersion and narrower size distribution of the nanoparticles. Although the presence of more surface oxides over the CoFeB catalysts as determined by XPS (shown below) may inhibit the aggregation of nanoparticles [24], the possibility that the ternary CoFeB alloys intrinsically have a lower surface energy than the CoB alloy cannot be ruled out.

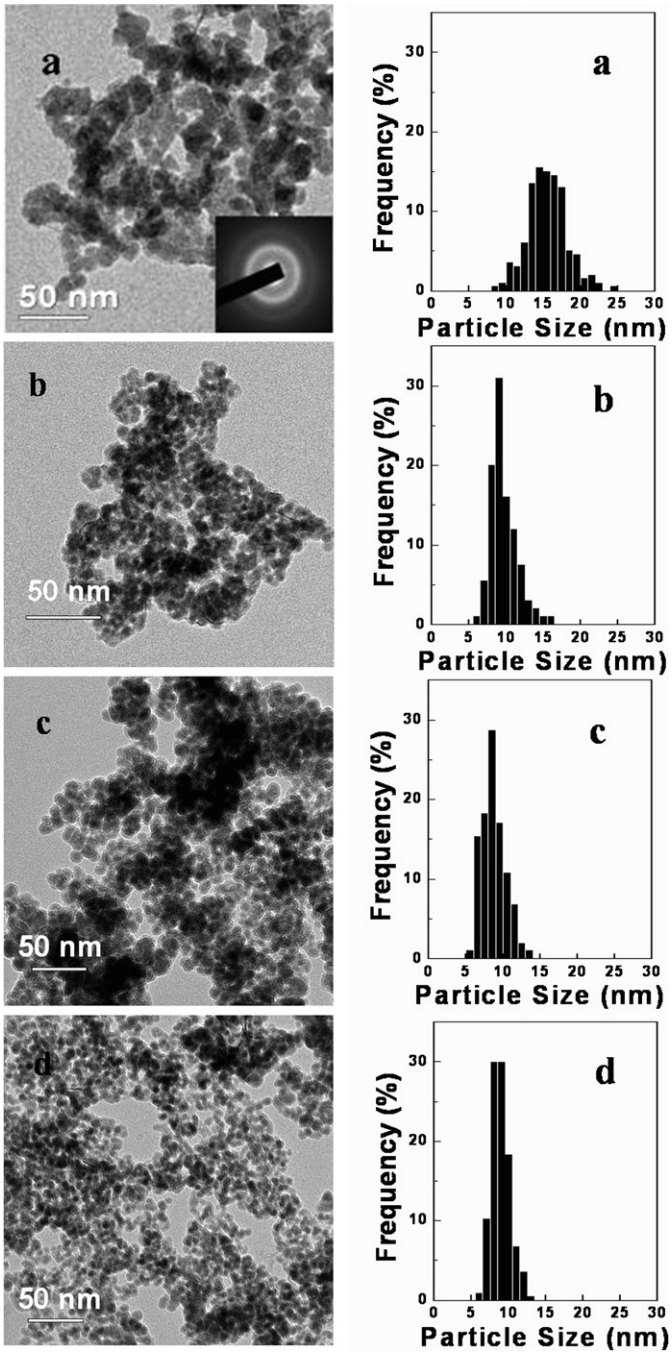

Fig. 1. TEM images and particle size distributions of the (a) CoB, (b) CoFeB-1, (c) CoFeB-2, and (d) CoFeB-3 catalysts. A typical SAED pattern for the catalysts is inserted in (a).

3.2. Bulk structure

The XRD patterns of the as-prepared catalysts exhibited only one broad peak at around 2θ of 45° with a full width at half maximum (FWHM) of 10° instead of sharp diffraction peaks. The SAED pattern shown in Fig. 1a demonstrates only a diffraction halo rather than distinct dots. Both of these patterns point to the amorphous structure of the CoB and CoFeB catalysts [9,25]. The amorphous nature of the CoB and CoFeB catalysts was further demonstrated by EXAFS. For all of the

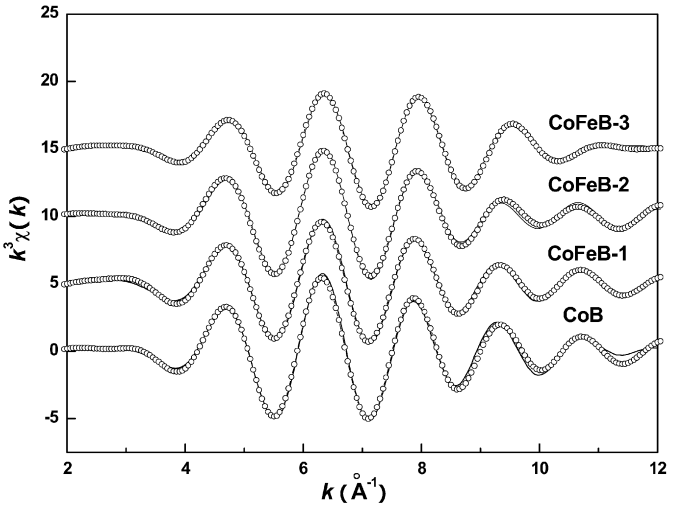

Fig. 2. Inverse Fourier transform of the first peak at the Co K-edge for the CoB and CoFeB catalysts using a two sub-shell approximation (—) and experimental data (○).

Table 2
Structural parameters from EXAFS on Co K-edge for the amorphous CoB and CoFeB alloy catalysts

Catalyst	Pair	N	R_0 (Å)	σ_T (Å)	σ_S (Å)	R_j (Å)[a]	ΔE_0 (eV)
CoB	Co–Co	10.7 ± 1.0	2.42 ± 0.02	0.081	0.247	2.67	−5.0
	Co–B	2.7 ± 0.4	2.05 ± 0.02	0.057	0.025	2.08	0.8
CoFeB-1	Co–(Co,Fe)	10.4 ± 1.0	2.42 ± 0.02	0.080	0.284	2.70	−5.0
	Co–B	2.7 ± 0.4	2.03 ± 0.02	0.056	0.027	2.06	0.8
CoFeB-2	Co–(Co,Fe)	10.4 ± 1.0	2.41 ± 0.02	0.080	0.293	2.70	−5.0
	Co–B	2.8 ± 0.3	2.03 ± 0.02	0.056	0.028	2.06	0.8
CoFeB-3	Co–(Co,Fe)	10.3 ± 1.0	2.39 ± 0.02	0.082	0.313	2.70	−5.0
	Co–B	2.7 ± 0.4	2.07 ± 0.02	0.056	0.027	2.10	0.8
Co foil	Co–Co	12	–	0.087	–	2.50	–

[a] Average interatomic distance $R_j = R_0 + \sigma_S$.

samples, the radial structure function (RSF) at the Co K-edge derived from the $k^3\chi(k)$ by Fourier transformation presented a single peak characteristic of amorphous metal–metalloid alloys [26].

The Co K-edge RSFs of the samples were inversely transformed to extract the structural parameters from the peak. Because Co and Fe can be considered as the same backscatterer [27], a two-shell approximation (i.e., Co–Co/Fe and Co–B subshells) was used for the fitting. This treatment is validated by the good quality of the simulated curves compared with the experimental data (Fig. 2). The structural parameters from the best fit, the nearest interatomic distance R_0, the average interatomic distance R_j, the coordination number N, the thermal disorder σ_T, the static disorder factor σ_S, and the energy shift ΔE_0 are summarized in Table 2. For the amorphous CoB catalyst, R_0 and N were 2.42 Å and 10.7 for the Co–Co subshell and 2.05 Å and 2.7 for the Co–B subshell. The nearest distance of Co–B was close to the sum of the covalent radii of Co and B ($1.16 + 0.88 = 2.04$ Å), whereas this distance was much shorter than the sum of the atomic radii of Co and B (2.32 Å). This

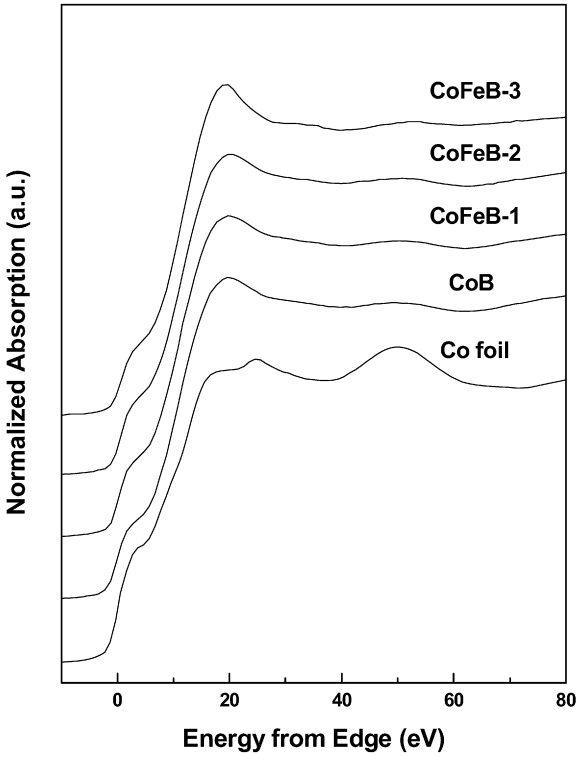

Fig. 3. Normalized Co K-edge XANES spectra for the Co foil and the CoB and CoFeB catalysts.

result is very similar to the findings for other metallic glasses [26–28], indicating the covalent character of the Co–B bond. Table 2 also reveals that within the error bar there were virtually no changes in the coordination number and interatomic distance for the Co–Co/Fe and Co–B subshells even when the bulk Fe content surpassed that of Co. This is reasonable because, as the size and electronic structure of the Fe and Co atoms are similar, Fe may isomorphously substitute for Co in the amorphous CoB alloy without noticeably changing the local environment around Co. A previous study also found that the interatomic distance of the Co–Co/Fe pair remained nearly constant with increasing Fe content in the amorphous $(Fe_xCo_{1-x})_{80}B_{20}$ alloys [29].

The Co K-edge XANES spectra of the samples are illustrated in Fig. 3. For all of the spectra, zero energy was selected at the inflection point of the threshold. In the spectra, the pre-edge peaks from about 0 to 10 eV are usually assigned to dipole transitions from 1s to the unoccupied final state originating from hybridized 3d and 4p orbitals with mainly 3d character, the intensities of which are strong functions of the local symmetry of the Co species [30]. Clearly, the Co XANES spectra of the four amorphous alloys are similar but are completely different from that of the Co foil. The close resemblance of the Co XANES spectra, combined with the nearly unchanged structural parameters in Table 2, strongly indicate that the metal atoms in the amorphous CoB and CoFeB alloys have identical local symmetry [31], which is also supported by the nearly unchanged Fe K-edge XANES spectra of the amorphous CoFeB and FeB alloys (not shown). Thus, the intensity of the pre-edge peak in Fig. 3 can provide a measure of the occupation of the 3d holes. From the figure, it can be determined that Co in the

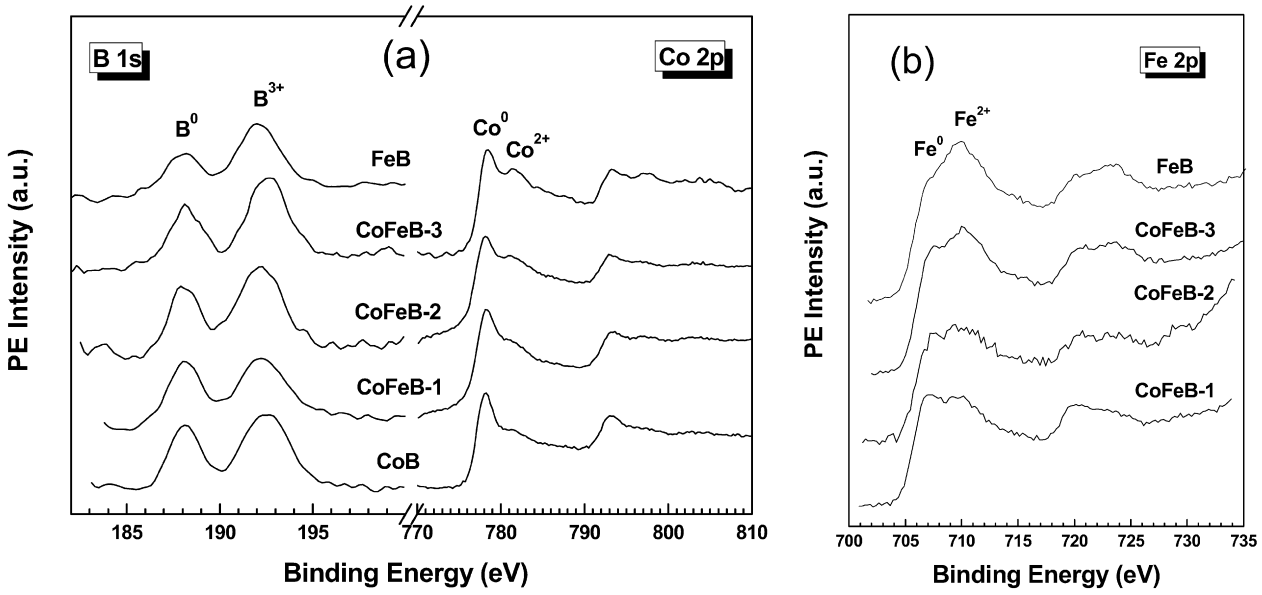

Fig. 4. XPS spectra of the B 1s, Co 2p, and Fe 2p levels of the CoB, CoFeB, and FeB catalysts.

amorphous alloys has similar 3d population irrespective of the Fe content.

It must be emphasized that a quantitative analysis of the XANES data requires complex calculations involving multiple scattering effects [32]. Nevertheless, the qualitative analysis of XANES allowed us to obtain important information about the effect of Fe on the structural and electronic properties of the amorphous CoB alloy.

3.3. Chemical state and surface composition

Fig. 4 shows the XPS spectra of the Co 2p, B 1s, and Fe 2p levels of the amorphous CoB, CoFeB, and FeB alloys. In Fig. 4a, most Co in the CoB catalyst was in the metallic state with a $2p_{3/2}$ BE of 778.0 eV, with a small portion of Co in the oxidized state with a $2p_{3/2}$ BE of 780.6 eV [33]. Similarly, for Fe in the CoFeB and FeB samples, both metallic Fe ($2p_{3/2}$ BE of 707.1 eV) and oxidized Fe ($2p_{3/2}$ BE of 709.8 eV) were identified [33], as shown in Fig. 4b. In Fig. 4a, besides elemental B with its 1s BE at 188.2 eV, oxidized B was observed with B 1s at 192.2 eV [33], due to the hydrolysis of BH_4^- during the reduction process in the aqueous solution [34].

Although no significant BE shifts of metallic Co and Fe were identified, the BE of elemental B in these amorphous alloys shifted about +1.2 eV relative to pure B [33]. A similar BE shift was recorded for amorphous NiB [12,24,35] and CoB alloys [18]. Based on Auger parameter measurements and primary and secondary features of the XPS spectra, Diplas et al. [36] proved that the positive 1s BE shift of elemental B was caused not by the final state effect [37], but rather by electron donation from B to Ni. The B 1s BE shift in the present case may be interpreted in the same manner.

Further inspection of Fig. 4 discloses that with the increment of Fe, the amount of oxidized species of Co, Fe, and B increased gradually. The curve-fitting results showing the relative amount of the elemental and oxidized species are listed in Table 3. Although the exact reason underlying the influence of Fe on the surface composition requires further investigation, the results were reproducible for samples prepared in separate runs.

Table 3
Curve-fitting results of Co 2p, B 1s, and Fe 2p XPS spectra for the CoB, CoFeB, and FeB catalysts (atomic percentages of the chemical species are given in the parentheses)

Catalyst	Co $2p_{3/2}$ (eV)	B 1s (eV)	Fe $2p_{3/2}$ (eV)
CoB	778.0 (70%)	188.2 (43%)	–
	780.6 (30%)	192.6 (57%)	–
CoFeB-1	777.9 (67%)	188.3 (35%)	707.0 (49%)
	780.6 (33%)	192.6 (65%)	709.3 (51%)
CoFeB-2	777.8 (67%)	188.2 (29%)	706.8 (45%)
	780.6 (33%)	192.6 (71%)	709.4 (55%)
CoFeB-3	777.8 (63%)	188.2 (25%)	707.1 (38%)
	780.6 (37%)	192.6 (75%)	709.8 (62%)
FeB	–	188.2 (21%)	706.9 (32%)
	–	192.6 (79%)	709.8 (68%)

3.4. Liquid-phase hydrogenation of crotonaldehyde

The time courses of liquid-phase hydrogenation of crotonaldehyde over the CoB and CoFeB catalysts are plotted in Fig. 5. The hydrogenation products of crotonaldehyde (CRAL) over these catalysts were butanal (BUAL) due to C=C bond hydrogenation, crotyl alcohol (CROL) due to C=O bond hydrogenation, and butanol (BUOL), the completely saturated product of secondary hydrogenation reactions. Moreover, a small amount of diacetal (1,1-diethoxybutane, DA) determined by GC-MS, was formed via a side reaction between butanal and the solvent ethanol, as depicted in Scheme 1. It should be mentioned that when CROL or BUAL was used as the reactant under the same hydrogenation condition as that of CRAL, further hydrogenation to BUOL rather than the isomerization between CROL and BUAL was observed.

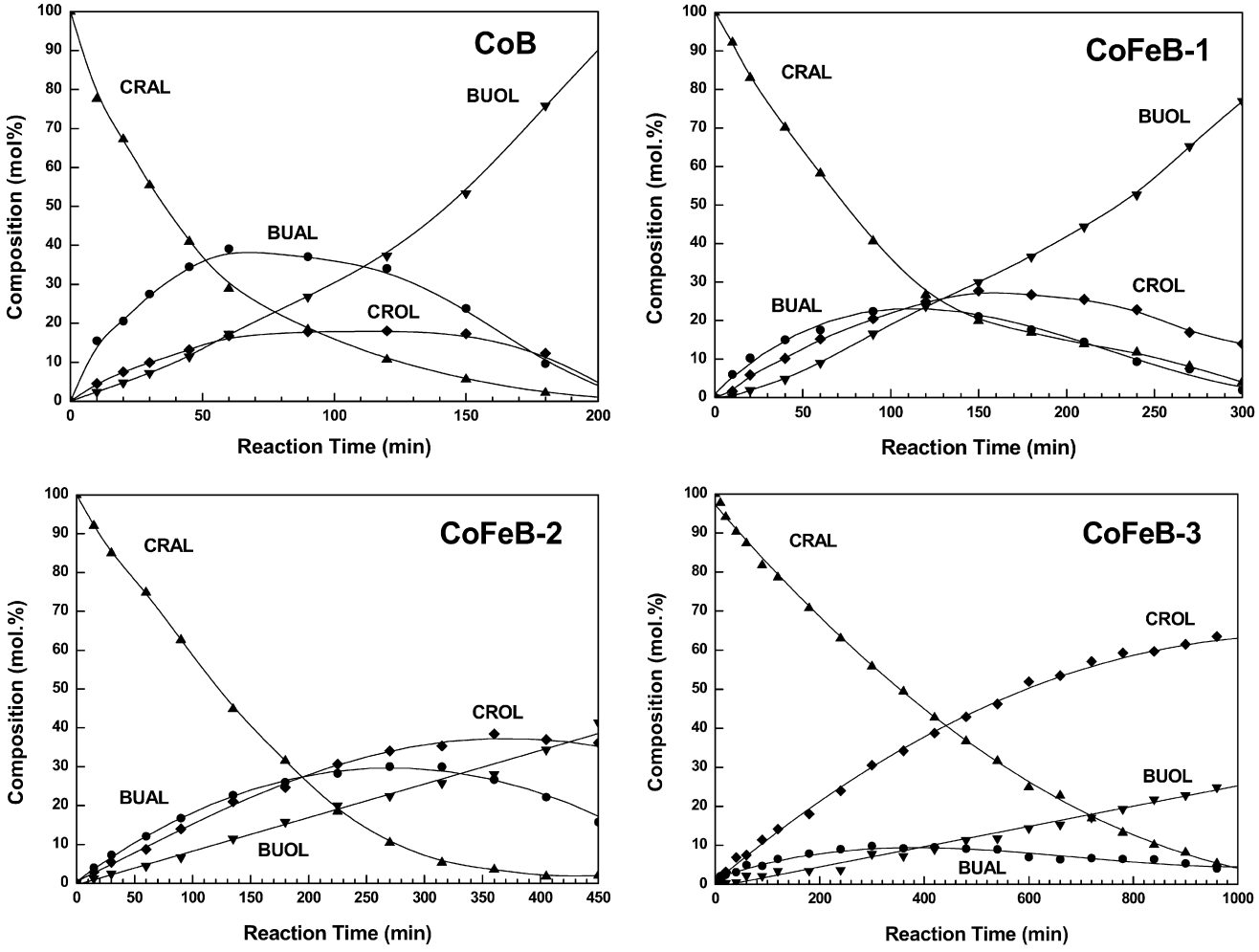

Fig. 5. Time dependences of crotonaldehyde hydrogenation over the CoB and CoFeB catalysts. Reaction conditions: $T = 373$ K, $P_{H_2} = 1.0$ MPa, crotonaldehyde/ethanol/$W_{cat} = 5.0$ ml/45.0 ml/0.50 g.

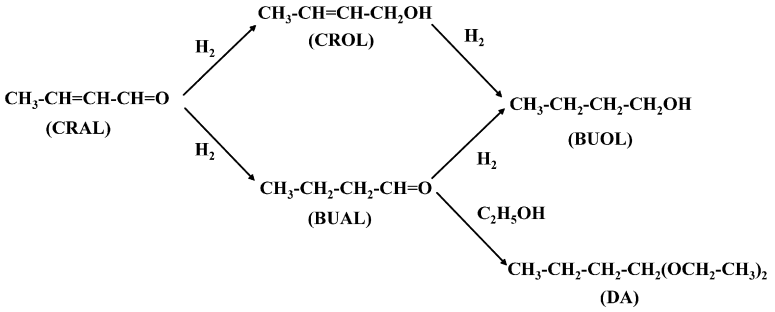

Scheme 1. Liquid-phase hydrogenation pathways of crotonaldehyde over the CoB and CoFeB catalysts.

Table 4 summarizes the product distribution corresponding to the maximum yield of crotyl alcohol over the CoB and CoFeB catalysts. Fe is remarkable in improving the selectivity to crotyl alcohol. Over the CoB catalyst without Fe, butanal formation was preferred over crotyl alcohol formation. The initial selectivity to crotyl alcohol (S_0) was 23%, and the maximum yield of crotyl alcohol was only 18%. Over the CoFeB-1 catalyst with ca. 20 mol% of Co replaced by Fe, S_0 drastically increased to 41%. S_0 amounted to 71% when the Fe/(Co + Fe) nominal ratio was 0.6, resulting in a crotyl alcohol yield as high as 63% over the CoFeB-3 catalyst.

An even higher Fe content did not lead to a higher crotyl alcohol yield. Over the CoFeB catalyst with Fe/(Co + Fe) nominal ratio of 0.8, the maximum yield of crotyl alcohol was <1% with crotonaldehyde conversion of 6% at a reaction time as long as 22 h. It is noteworthy that no hydrogenation product was detected when the amorphous FeB alloy was used as the catalyst, demonstrating that Fe was not the active center for the reaction.

The extrapolated consumption rates of crotonaldehyde at zero conversion (r_{CRAL}), as an indication of the activity of the catalysts, are listed in Table 4. Different from the promoting effect of Fe on the selectivity, Fe was always detrimental to the

Table 4
The hydrogenation results of crotonaldehyde over the CoB and CoFeB catalysts

Catalyst	t[a] (h)	Conversion[a] (%)	S[a] (%)				Y_{CROL}[a] (%)	S_0 (%)	r_{CRAL}[b]	$r_{C=O}$[b]	$r_{C=C}$[b]
			CROL	BUAL	BUOL	DA					
CoB	2.0	89	20	38	42	0	18	23	1.25	0.29	0.89
CoFeB-1	2.5	80	35	26	37	2	28	41	0.54	0.18	0.29
CoFeB-2	6.0	94	41	27	29	3	38	45	0.32	0.11	0.15
CoFeB-3	16.0	95	67	26	4	3	63	71	0.10	0.07	0.03

[a] Values corresponding to the maximum yield of crotyl alcohol.
[b] Unit in mmol min^{-1} g_{cat}^{-1}.

activity of the CoB catalyst in crotonaldehyde hydrogenation. As inferred by XPS, the continuously decreasing r_{CRAL} can be partly associated with the increasing presence of surface oxides of Co, Fe, and B on the catalysts at higher Fe content, leading to lower total metal surface area (S_H, Table 1) available for the reaction. The presence of more catalytically inactive metallic Fe atoms on the surface, even though they also contribute to S_H, is another important factor responsible for the decreased activity.

3.5. Modification mechanism of Fe

To gain insight into the role of Fe in enhancing the selectivity toward crotyl alcohol over the CoB catalyst, knowledge about the variation of the formation rates of butanal ($r_{C=C}$) and crotyl alcohol ($r_{C=O}$) extrapolated to zero conversion against the Fe content is necessary. These data are also given in Table 4. For the CoB catalyst, $r_{C=C}$ was 0.89 mmol min^{-1} g_{cat}^{-1} and $r_{C=O}$ was 0.29 mmol min^{-1} g_{cat}^{-1}, which readily accounted for the low selectivity and consequently the low yield of crotyl alcohol on the catalyst. Fe did not improve the selectivity to crotyl alcohol by increasing $r_{C=O}$; rather, it simultaneously reduced $r_{C=C}$ and $r_{C=O}$, but the extent of reduction of the former was about one order of magnitude more than that of the latter. Over the CoFeB-3 catalyst, the $r_{C=C}/r_{C=O}$ ratio was reversed, resulting in a high crotyl alcohol yield.

We further expressed the formation rates of butanal and crotyl alcohol by dividing $r_{C=C}$ and $r_{C=O}$ by the number of the active sites measured by H_2-TPD; the results are designated $TOF_{C=C}$ and $TOF_{C=O}$, respectively. With the fact that Fe was inactive for the reaction in mind, the contribution of Fe was excluded from the total metal surface area, S_H, by assuming that its contribution was proportional to the surface $Fe^0/(Co^0 + Fe^0)$ atomic ratio as determined by XPS. Fig. 6 shows the evolutions of $TOF_{C=C}$ and $TOF_{C=O}$ as a function of the surface $Fe^0/(Co^0 + Fe^0)$ ratio. Although the possible hydrogen consumption during the TPD run due to the presence of oxides would underestimate the number of active sites and thus overestimate the values of $TOF_{C=C}$ and $TOF_{C=O}$, the decrement of $TOF_{C=C}$ is known to be much faster than that of $TOF_{C=O}$.

Previous studies have proposed two mechanisms to account for the promoting effect of a second metal on the selectivity over bimetallic catalysts in α,β-unsaturated aldehyde hydrogenation [1–3]: In the first of these mechanisms, the second metal or its oxide functions as electrophilic or Lewis acid sites for the adsorption and activation of the C=O bond via the electron lone pair on oxygen. In the second mechanism, the second

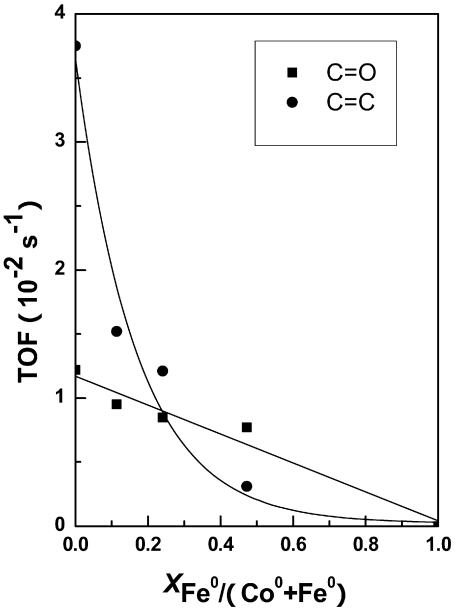

Fig. 6. The evolutions of the intrinsic formation rates of butanal and crotyl alcohol against the surface $Fe^0/(Co^0 + Fe^0)$ atomic ratio in the CoB and CoFeB catalysts.

metal functions as an electron-donating ligand, increasing the electron density on the active metal, thus decreasing the binding energy of the C=C bond in particular and favoring the hydrogenation of C=O with respect to C=C. The first mechanism favors enhanced selectivity by increasing the activation of the C=O bond; the second, by decreasing the activation of the C=C bond [2].

On the CoB and CoFeB catalysts, XPS revealed increased amounts of oxidized Co, Fe, and B species with increasing Fe content. The surface oxides might act following the first mechanism to enhance the selectivity to crotyl alcohol [19]. However, Fig. 6 does not show the expected increment of $TOF_{C=O}$ characteristic of the first mechanism, and so this mechanism can be disregarded. On the other hand, although the $TOF_{C=C}$ in Fig. 6 decreased with the increment of Fe, the invariant BEs of Co 2p, Fe 2p, and B 1s, the identical Co K-edge XANES features, as well as the similar electronegativities of Fe and Co, strongly disfavor a ligand or an electronic effect of Fe on Co.

We tentatively attribute the Fe's modifying effect on the selectivity to crotyl alcohol to the ensemble size effect. According to Ponec's review of alloy catalysts [37], for a binary alloy AB, in which metal A is very active in both reactions while B is vir-

tually inactive and no electron transfer occurs between the alloy components, if the areal activity of the alloy catalyst decreases linearly with the B content in the surface, then it is insensitive to ensemble size. If the areal activity decreases nonlinearly with the B content, then it is interpreted as being sensitive to ensemble size. As for the CoFeB catalysts, the much faster decrease in $TOF_{C=C}$ can be similarly interpreted as demonstrating that the hydrogenation of the C=C bond in crotonaldehyde requires a larger ensemble of contiguous metallic Co atoms (sensitive to ensemble size), whereas the much more slowly decreasing of $TOF_{C=O}$ can be interpreted as indicating that the hydrogenation of the C=O bond in crotonaldehyde requires a smaller ensemble size.

It is acknowledged that the relative accessibility and the binding strength of C=C and C=O in α,β-unsaturated aldehydes to the catalyst surface are decisive to the selectivity [3,7]. The preferential binding through C=O, in either the η_1-on top or the η_2-di-$\sigma_{C=O}$ adsorption mode, should favor a high selectivity to unsaturated alcohols in α,β-unsaturated aldehyde hydrogenation [3], whereas α,β-unsaturated aldehydes in the tightly binding η_4-di-π adsorption mode is the potential cause of low selectivity to unsaturated alcohols, as the production of saturated aldehydes is favored for kinetic reasons [4,38,39]. We suppose that the competition between the η_1-on top or η_2-di-$\sigma_{C=O}$ mode and the η_4-di-π mode is also present on the CoB and CoFeB catalysts, which determines the selectivity. The tilted η_1-on top or the η_2-di-$\sigma_{C=O}$ mode leading to crotyl alcohol is expected to occupy fewer contiguous Co atoms than the more planar η_4-di-π mode. Consequently, the former is less affected when the catalytically inactive Fe is incorporated into the CoB catalyst, that is, it is less sensitive to the ensemble size. This argument can rationalize the evolution of the $TOF_{C=C}$ and $TOF_{C=O}$ with respect to the Fe content displayed in Fig. 6.

4. Conclusion

In liquid-phase hydrogenation of crotonaldehyde, incorporation of the inactive Fe into the amorphous CoB alloy catalyst is an effective way to improve the selectivity to crotyl alcohol. Over the best CoFeB-3 catalyst, the initial selectivity was as high as 71%, and the maximum yield of crotyl alcohol reached 63%. Based on the characterizations and previous findings, we conclude that the presence of more surface oxides or the ligand effect of Fe is unlikely to account for selectivity enhancement. The evolutions of the intrinsic formation rates of butanal and crotyl alcohol strongly suggest that the modification mechanism of Fe can be attributed to the ensemble size effect.

Acknowledgments

This work was supported by the National Basic Research Program of China (grant 2006CB202502), Shanghai Science and Technology Committee (grant 06JC14009), the Fok Ying Tong Education Foundation (grant 104022), the National Science Foundation of China (grants 20673025 and 20421303), the Beijing Synchrotron Radiation Facility, and the Synchrotron Radiation Center of Fudan University.

References

[1] M. Bartók, Á. Molnár, in: S. Patai (Ed.), The Chemistry of Double-Bonded Functional Groups, Suppl. A3, Wiley, New York, 1997, chap. 16.
[2] P. Gallezot, D. Richard, Catal. Rev. Sci. Eng. 40 (1998) 81.
[3] V. Ponec, Appl. Catal. A 149 (1997) 27.
[4] F. Delbecq, P. Sautet, J. Catal. 152 (1995) 217.
[5] P. Concepción, A. Corma, J. Silvestre-Albero, V. Franco, J.Y. Chane-Ching, J. Am. Chem. Soc. 126 (2004) 5523.
[6] P. Beccat, J.C. Bertolini, Y. Gauthier, J. Massardier, P. Ruiz, J. Catal. 126 (1990) 451.
[7] T.B.L.W. Marinelli, S. Nabuurs, V. Ponec, J. Catal. 151 (1995) 431.
[8] F. Delbecq, P. Sautet, J. Catal. 165 (1996) 152.
[9] J.V. Wonterghem, S. Morup, J.W. Christion, S. Charles, W.S. Wells, Nature 322 (1986) 622.
[10] A. Baiker, Faraday Discuss. Chem. Soc. 87 (1989) 239.
[11] Á. Molnár, M. Bartók, G.V. Smith, Adv. Catal. 36 (1989) 329.
[12] J.F. Deng, H.X. Li, W.J. Wang, Catal. Today 51 (1999) 113.
[13] Y. Nitta, T. Imanaka, S. Teranishi, Bull. Chem. Soc. Jpn. 53 (1980) 3154.
[14] Y.Z. Chen, K.J. Wu, Appl. Catal. 78 (1991) 185.
[15] H.X. Li, X.F. Chen, M.H. Wang, Y.P. Xu, Appl. Catal. A 225 (2002) 117.
[16] X.F. Chen, H.X. Li, H.S. Luo, M.H. Qiao, Appl. Catal. A 233 (2002) 13.
[17] Y. Pei, J. Fang, H.R. Hu, J.H. Zhuang, K.N. Fan, H.X. Li, M.H. Qiao, Acta Chim. Sinica 63 (2005) 289.
[18] Y. Pei, H.R. Hu, J. Fang, M.H. Qiao, W.L. Dai, K.N. Fan, H.X. Li, J. Mol. Catal. A 15 (2004) 243.
[19] Y. Pei, J.Q. Wang, Q. Fu, P.J. Guo, M.H. Qiao, S.R. Yan, K.N. Fan, New J. Chem. 29 (2005) 992.
[20] R.C. Reuel, C.H. Bartholomew, J. Catal. 85 (1984) 63.
[21] B. Lengeler, P. Eisenberger, Phys. Rev. B 21 (1980) 4507.
[22] M. De Crescenzi, A. Balsatori, F. Comin, L. Incoccia, S. Mobilio, N. Motta, Solid State Commun. 37 (1981) 921.
[23] A. Ankudinov, B. Ravel, J.J. Rehr, FEFF8, version 8.20, University of Washington, Seattle, WA, 2002.
[24] J. Fang, X.Y. Chen, B. Liu, S.R. Yan, M.H. Qiao, H.X. Li, H.Y. He, K.N. Fan, J. Catal. 229 (2005) 97.
[25] T. Osaka, K. Arai, N. Masubuchi, Y. Yamazaki, T. Namikawa, Jpn. J. Appl. Phys. 28 (1989) 866.
[26] S.Q. Wei, H. Oyanagi, Z.R. Li, X.Y. Zhang, W.H. Liu, S.L. Yin, X.G. Wang, Phys. Rev. B 63 (2001) 224201.
[27] M.L. Fdez-Gubieda, I. Orúe, F. Plazaola, J.M. Barandiarán, Phys. Rev. B 53 (1996) 620.
[28] S.J. Gurman, J. Mater. Sci. 17 (1982) 1541.
[29] I. Orue, M.L. Fdez-Gubieda, F. Plazaola, J. Non-Cryst. Solids 287 (2001) 75.
[30] E.K. Hlil, R. Baudoing-Savois, B. Moraweck, A.J. Renouprez, J. Phys. Chem. 100 (1996) 3102.
[31] J.C.J. Bart, Adv. Catal. 34 (1986) 203.
[32] P.J. Durham, in: D.C. Koningsberger, R. Prins (Eds.), X-Ray Absorption: Principles, Applications, Techniques of EXAFS, SEXAFS and XANES, Wiley, New York, 1988, chap. 2.
[33] J.F. Moulder, W.F. Stickle, P.E. Sobol, K.D. Bomben, in: J. Chastain (Ed.), Handbook of X-Ray Photoelectron Spectroscopy, Perkin-Elmer, Eden Prairie, MN, 1992.
[34] Y. Chen, Catal. Today 44 (1998) 3.
[35] H. Li, H.X. Li, W.L. Dai, W.J. Wang, Z.G. Fang, J.F. Deng, Appl. Surf. Sci. 152 (1999) 25.
[36] S. Diplas, J. Lehrmann, S. Jørgensen, T. Våland, J. Taftø, Philos. Mag. 85 (2005) 981.
[37] V. Ponec, Appl. Catal. A 222 (2001) 31.
[38] D. Loffreda, F. Delbecq, F. Vigné, P. Sautet, Angew. Chem. Int. Ed. 44 (2005) 5279.
[39] D. Loffreda, F. Delbecq, F. Vigné, P. Sautet, J. Am. Chem. Soc. 128 (2006) 1316.